Paper

Full-vectorial analysis of connection problem in optical fiber

Non-member Tokuo Miyamoto (Fukuoka University)
Non-member Michiko Momoda (Fukuoka University)
Member Kiyotoshi Yasumoto (Kyushu University)

In the connection of two optical fibers, higher-order modes appear occasionally even for slight shift of the two fibers. In usual fiber, four higher-order modes, TE_{01}, TM_{01} and two of HE_{21} modes, have slightly different eigenvalues and field distributions of two-lobe patterns described by linearly polarized E_x and E_y, respectively. Then in order to investigate precisely the occurrence mechanism of such higher-order modes, accurate full-vectorial numerical method is required. In this paper, Fourier series expansion method is applied to the full-vectorial analysis of the connection problem. First, the eigenvalues and the field distributions of the four higher-order modes in step-index type optical fibers are computed by the method, and their accuracies are examined. Then the occurrence mechanism of the higher-order modes caused by the transverse shift of the two fibers is made clear.

Keywords: full-vectorial analysis, field distribution, higher-order mode, optical fiber, connection problem

1. Introduction

Development of optical communication system increases the chance of connection of optical fibers. Such a connection becomes a cause of occurrence of higher-order modes even for slight shift between two fibers. In practical weakly guiding fiber, there is the case where the first higher-order mode LP_{11} can propagate. This LP_{11} mode is defined under the approximation of small refractive index difference Δn between core and cladding, and includes approximately degenerated TE_{01}, TM_{01} and two of HE_{21} modes which have slightly different eigenvalues, and their fields are described by two-lobe patterns of linearly polarized E_x and E_y, respectively[1]~[3]. For a step-index type optical fiber, exact solutions can be obtained by using cylindrical coordinate system[1],[3]. However, for the precise analysis of the connection problem in which reflected and radiation fields are included and the concerned higher-order modes are in approximate degeneracy, efficient full-vectorial numerical method is required.

The authors have applied a Fourier series expansion method[5]~[7], in which virtual periodicity in both transverse directions is introduced, to full-vectorial analyses of arbitrary three-dimensional waveguide system[8]~[11]. In the method, Maxwell's equations are lead to a set of linear equations for vectorized Fourier coefficients in which any derivatives of permittivity of the medium are not included. The solutions yield the full-vectorial fields for the guided and discretized radiation modes, propagating both in forward and backward directions, even in the case of larger Δn. The accuracy of the solution can be improved by increasing the truncation number of the Fourier expansions, and has been investigated in Ref. (9).

In this paper, we apply our method in order to make clear the connection problem between the two step-index optical fibers. First, the eigenvalues and the field distributions described by linearly polarized E_x and E_y are computed numerically for HE_{11}, TE_{01}, TM_{01} and two of HE_{21} modes in the two typical fibers of Δn=0.6% (in approximate degeneracy) and Δn=10% (not in degeneracy). The accuracies of those results are examined. Then the occurrence mechanism of the higher-order modes in the output fiber is made clear for the transverse shifts along x- and y-axes and the oblique axis titled by 45 degree between the two fibers.

2. Formulation of the method

First, we formulate our method for full-wave Fourier modal analysis on the guided and discretized radiation modes propagating both in forward and backward directions along three-dimensional waveguide system.

In this paper we assume $\exp(j\omega t)$ where ω is angular frequency of the incident wave. For convenience, we normalize the coordinate variables by multiplying wave number $k_0(=\omega\sqrt{\varepsilon_0\mu_0})$ in free space, the electric fields $(\varepsilon_0/\mu_0)^{1/4}$, and the magnetic field $(\mu_0/\varepsilon_0)^{1/4}$, respectively. ε_0 and μ_0 are permittivity and permeability in free space, respectively. Then the normalized electric and magnetic fields satisfy the following Maxwell's equations :

$$\nabla\times\mathbf{E}(x,y,z) = -j\,\mathbf{H}(x,y,z) \quad \cdots(1)$$

$$\nabla\times\mathbf{H}(x,y,z) = j\,\varepsilon(x,y)\mathbf{E}(x,y,z) \quad \cdots(2)$$

where $\varepsilon(x,y)$ includes the whole relative permittivities in the cross section of the waveguide system. To solve Eqs. (1) and (2) by the Fourier series expansion method, we introduce a virtual periodic boundaries with the periods Λ_x and Λ_y in the x and y directions as shown in Fig.1. Then original waveguide structure is approximated in terms of one period of the periodic waveguide arrays. For the assumed structure, each component of the electro-magnetic field is approximated by the following truncated double Fourier series expansion :

$$E_\nu(x,y,z) = \sum_{m=-M}^{M}\sum_{n=-N}^{N} e^\nu_{m,n}\exp(-jsmx)\exp(-jtny) \quad \cdots(3)$$

$$H_\nu(x,y,z) = \sum_{m=-M}^{M}\sum_{n=-N}^{N} h^\nu_{m,n}\exp(-jsmx)\exp(-jtny) \quad \cdots(4)$$

where $\nu = x,y,z$, $s = 2\pi/\Lambda_x$, $t = 2\pi/\Lambda_y$, m and n are integers. Here, the larger magnitude of $\Lambda_x(=\Lambda_y)$ is better in order to neglect the reflected fields from the virtual boundaries. However, for larger $\Lambda_x(=\Lambda_y)$, larger M(=N) is needed to maintain a certain accuracy. According to our experience, the magnitude of $\Lambda_x(=\Lambda_y)$ larger than 3~4 times of the diameter of the waveguide is seemed to be enough.

Eqs. (3) and (4) are substituted into Eqs. (1) and (2). Then the resulting equations are multiplied by $\exp(jsm'x)\exp(jtn'y)/\Lambda_x\Lambda_y$ and integrated over $0\le x\le\Lambda_x$ and $0\le y\le\Lambda_y$. Using the orthogonality of the complex Fourier series, these are lead to a set of linear differential equations in vectorial form for the transverse expansion coefficients $\{e^\nu_{m,n}(z)\}$, and $\{h^\nu_{m,n}(z)\}$ (ν=x,y) as follows :

$$\frac{d}{dz}\mathbf{h}(z) = -j\,\mathbf{C}_1\mathbf{e}(z) \quad \cdots(5)$$

$$\frac{d}{dz}\mathbf{e}(z) = -j\,\mathbf{C}_2\mathbf{h}(z) \quad \cdots(6)$$

$$\mathbf{e}(z) = [\mathbf{e}^x(z)\ \mathbf{e}^y(z)]^t,\quad \mathbf{h}(z) = [\mathbf{h}^x(z)\ \mathbf{h}^y(z)]^t \quad \cdots(7)$$

$$\mathbf{e}^\nu(z) = [e^\nu_{-M,-N}\ \cdots\ e^\nu_{-M,N}\ \cdots\ e^\nu_{M,-N}\ \cdots\ e^\nu_{M,N}]^t \quad \cdots(8)$$

$$\mathbf{h}^\nu(z) = [h^\nu_{-M,-N}\ \cdots\ h^\nu_{-M,N}\ \cdots\ h^\nu_{M,-N}\ \cdots\ h^\nu_{M,N}]^t \quad \cdots(9)$$

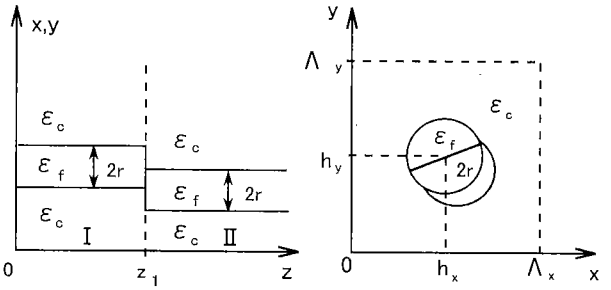

(a) (b)

Fig.1. Connection of two fields (a) and first period of virtual periodic array (b).

$$\mathbf{C}_1 = \begin{bmatrix} -\mathbf{NM} & \mathbf{M}^2-\mathbf{A} \\ -\mathbf{N}^2+\mathbf{A} & \mathbf{NM} \end{bmatrix} \quad \cdots(10)$$

$$\mathbf{C}_2 = \begin{bmatrix} \mathbf{MA}^{-1}\mathbf{N} & -\mathbf{MA}^{-1}\mathbf{M}+\mathbf{I} \\ \mathbf{NA}^{-1}\mathbf{N}-\mathbf{I} & -\mathbf{NA}^{-1}\mathbf{M} \end{bmatrix} \quad \cdots(11)$$

where I is unit matrix of order K (K=(2M+1)(2N+1)). The diagonal matrices **M** and **N** of order K are defined by

$$\mathbf{M} = [\,sm\delta_{mm'}\delta_{nn'}\,],\quad \mathbf{N} = [\,tn\delta_{mm'}\delta_{nn'}\,] \quad \cdots(12)$$

respectively, where $\delta_{mm'}$ is the Kroneker's delta. s,m,t and n are defined in Eqs.(3) and (4). **A** is a cyclic matrix of order K which consists of the double Fourier components of $\varepsilon(x,y)$ as follows :

$$\mathbf{A} = [\,\varepsilon_{p,q}\,],\quad p = m-m',\quad q = n-n' \quad \cdots(13)$$

$$\varepsilon_{p,q} = \frac{1}{\Lambda_x\Lambda_y}\int_0^{\Lambda_y} dy\int_0^{\Lambda_x} dx\ \varepsilon(x,y)\exp(-jspx)\exp(-jtqy)\,. \quad \cdots(14)$$

The superscript "t" in Eqs. (7)~(9) indicates transpose of vectors.

The solution of Eqs. (5) and (6) is obtained by solving directly the following eigenvalue problem of matrix **C** of order 2K :

$$\frac{d^2}{dz^2}\mathbf{e}(z) = -\mathbf{C}\,\mathbf{e}(z),\quad \mathbf{C} = \mathbf{C}_2\mathbf{C}_1 \quad \cdots(15)$$

$\mathbf{h}(z)$ is obtained from the solution of Eq. (15) using Eq. (6). Then using standard calculational subroutine we can easily obtain eigenvalues κ_k and associated eigenvectors $\mathbf{P}^e_k$ (k=1,2,$\cdots$,2K) of matrix **C**. It is noted that quite same solution can be obtained using the similar equation for $\mathbf{h}(z)$ instead of $\mathbf{e}(z)$ in Eq. (15), because we solve Maxwell's equation itself.

Introducing a new vectorial function $\mathbf{a}(z)$ of order 2K which satisfy

$$\mathbf{e}(z)=\mathbf{P}^{e}\mathbf{a}(z),\quad \mathbf{P}^{e}=[\,\mathbf{P}_1^{e},\ \mathbf{P}_2^{e},\ \cdots\cdots,\mathbf{P}_{2K}^{e}\,] \qquad \cdots(16)$$

solution of Eq. (15) is obtained as follows :

$$\mathbf{e}(z)=[\mathbf{P}^{e}\ \mathbf{P}^{e}]\cdot\begin{bmatrix}\exp(-j\sqrt{\kappa_k}(z-z_0))\delta_{kk'} & \mathbf{0}\\ \mathbf{0} & \exp(j\sqrt{\kappa_k}(z-z_0))\delta_{kk'}\end{bmatrix}\begin{bmatrix}\mathbf{a}^{+}(z_0)\\ \mathbf{a}^{-}(z_0)\end{bmatrix} \qquad \cdots(17)$$

$$\mathbf{a}^{\pm}=[a_1^{\pm},\ a_2^{\pm},\ \cdots\cdots,a_{2K}^{\pm}]^{t} \qquad \cdots(18)$$

Here the bracket [ ] in Eq. (17) indicates a diagonal matrix of order 4K and $a_k^{\pm}$ is a complex mode amplitude of k-th eigenmode propagating in the $\pm z$ direction, respectively, and normalized propagation constant is $\pm\sqrt{\kappa_k}\ (=\pm\beta_k/k_0)$. Here we assume $\mathrm{Re}\sqrt{\kappa_k}\geq 0$ and $\mathrm{Im}\sqrt{\kappa_k}<0$. The k-th mode satisfying $\left|\sqrt{\kappa_k}\right|>\sqrt{\varepsilon_c}$ is the guided mode and the case $\left|\sqrt{\kappa_k}\right|<\sqrt{\varepsilon_c}$ is the discretized radiation mode. In the case where $\sqrt{\kappa_k}$ is imaginary, the wave is evanescent and attenuates along +z-direction. $\mathbf{h}(z)$ can be obtained by differentiating $\mathbf{e}(z)$ from Eqs. (6) and (17). Thus electric and magnetic fields can be obtained by substituting each component of

$$\mathbf{f}(z)=[\mathbf{e}(z)\ \mathbf{h}(z)]^{t} \qquad \cdots(19)$$

into Eqs. (3) and (4) for each normalized propagation constant $\sqrt{\kappa_k}$ in the k-th mode. The eigenvector $\mathbf{P}_k^{e}$ is normalized so that the power carried by the respective k-th mode equals to $|a_k|^2$.

3. Application to the connection problem

Next, we apply the method to the connection problem as shown in Fig.1. That is, a dominant mode is incident from region I to region II . Expansion coefficients in each region are expressed in vectorial form as $\mathbf{f}^{i}(z)$ (i = I , II), by referring Eqs. (6), (17) and (19), respectively. Eigenvalues, eigenvectors and complex amplitude vectors in each region are expressed as $\sqrt{\kappa_k^{i}}$, $\mathbf{P}^{i}$ and $\mathbf{a}^{i}(z)$ (i= I , II), respectively. Here

$$\mathbf{P}^{i}=\begin{bmatrix}\mathbf{P}^{e} & \mathbf{P}^{e}\\ \mathbf{P}^{h} & -\mathbf{P}^{h}\end{bmatrix}=\begin{bmatrix}\mathbf{P}^{i+} & \mathbf{P}^{i-}\end{bmatrix},\quad \mathbf{P}^{h}=\sqrt{\kappa_k}\ \mathbf{C}_2^{-1}\mathbf{P}^{e} \qquad \cdots(20)$$

Then the boundary conditions for transverse electric and magnetic fields at $z=z_1$ are satisfied by

$$\mathbf{f}^{I}(z_1)=\mathbf{f}^{II}(z_1). \qquad \cdots(21)$$

As initial conditions, we consider the incidence of dominant mode from z=0 in region I and no reflection in the region II due to the assumption of semi-infinite waveguide. That is,

$$\mathbf{a}^{I+}(0)=[1,0,\cdots,0]^{t},\quad \mathbf{a}^{II-}(z_1)=\mathbf{0} \qquad \cdots(22)$$

From Eqs. (21) and (22) , following equation is lead :

$$\begin{bmatrix}\mathbf{a}^{II+}(z_1)\\ \mathbf{a}^{I-}(0)\end{bmatrix}=\begin{bmatrix}\mathbf{P}^{II+} & \mathbf{P}^{I-'}\end{bmatrix}^{-1}\mathbf{P}_1^{I+}\exp(-j\sqrt{\kappa_1^{I}}\ z_1), \qquad \cdots(23)$$

$$\mathbf{P}^{I-'}=\mathbf{P}^{I-}[\exp(j\sqrt{\kappa_1^{I}}\ z_1)\delta_{kk'}]$$

Then the solutions $\mathbf{a}^{II+}(z_1)$ and $\mathbf{a}^{I-}(0)$ are obtained from Eq. (23). The transmitted total powers of guided and discretized radiation modes are expressed as

$$T_g=\sum_{k=1}^{K_2}\left|a_k^{II+}(z_1)\right|^2,\quad T_r=\sum_{k=K_2+1}^{K}\left|a_k^{II+}(z_1)\right|^2 \qquad \cdots(24)$$

and the reflected total powers as

$$R_g=\sum_{k=1}^{K_1}\left|a_k^{I-}(0)\right|^2,\quad R_r=\sum_{k=K_1+1}^{K}\left|a_k^{I-}(0)\right|^2 \qquad \cdots(25)$$

respectively. Here $T_g+T_r+R_g+R_r=1$, and K_1 and K_2 are the numbers of guided modes in the waveguides of region I and region II, respectively.

4. Numerical results

4.1 Eigenvalues and field distributions of eigenmodes Electrical field lines and intensity patterns of eigenmodes in a weakly guiding step-index type optical fiber are described briefly in Fig.2[(1)~(3)]. First higher-order mode LP_{11} includes so called TE_{01}, TM_{01}, HE_{21}^{M} and HE_{21}^{E} modes, which degenerate approximately, and their field intensities are described by the two-lobe patterns of E_x and E_y, respectively, as shown in Fig.2. In this paper, HE_{21}^{M} and HE_{21}^{E} indicate two of HE_{21} modes which have the similar two-lobe pattern of E_x (E_y) as TM_{01} and TE_{01} modes, respectively. As such modes do not degenerate perfectly, even in actual weakly guiding fiber, the eigenvalues are slightly different, according to the degree of degeneracy. For larger Δn, which is not in degeneracy, those four modes also have the similar two-lobe patterns of E_x and E_y, as shown in Fig.2.

In order to investigate such modes, proposed full-

mode	LP_{01}		LP_{11}			
	HE_{11}^{y}	HE_{11}^{x}	TE_{01}	TM_{01}	HE_{21}^{M}	HE_{21}^{E}
electric vector						
field pattern E_x						
field pattern E_y						
mode number	①	②	③	④	⑤	⑥

Fig.2. Eigenmode and field pattern of weakly guiding optical fiber[(2),(3)] .

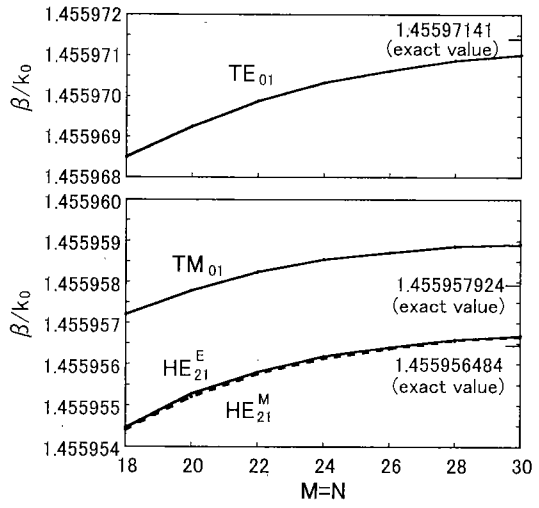

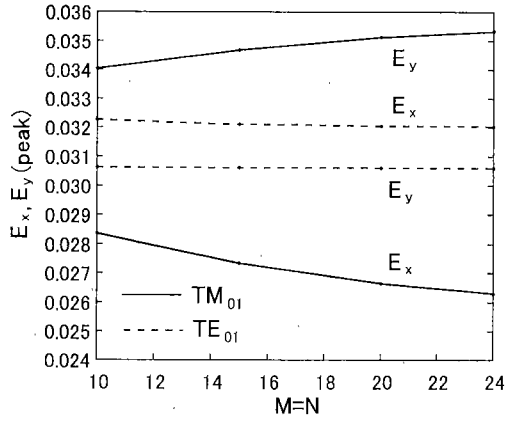

(a) $\Delta n=0.6\%$, $\Lambda_x = \Lambda_y = 30\lambda$

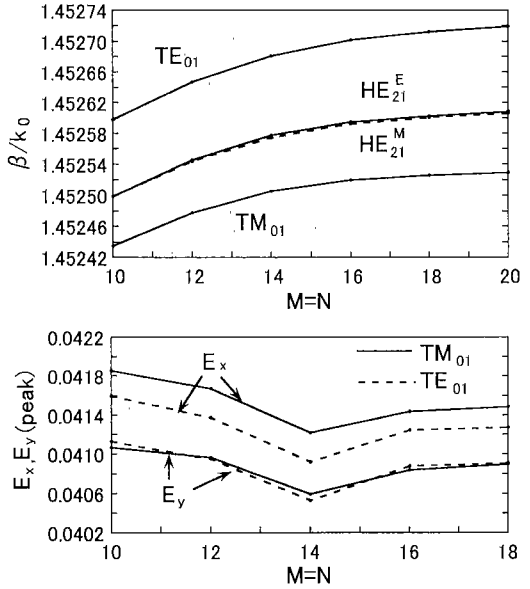

(b) $\Delta n=10\%$, $\Lambda_x = \Lambda_y = 20\lambda$

Fig.3. Convergency of eigenvalue and field distribution when truncation number M(=N) is increased

vectorial numerical method is applied for a step-index type optical fiber with the core of radius $r=3.46\lambda$ and refractive index $\sqrt{\varepsilon_f}=1.462$, surrounded by the cladding $\sqrt{\varepsilon_c}=1.453$ ($\Delta n=0.6\%$ as the case of weakly guiding fiber) and 1.3158 ($\Delta n=10\%$ as the case on no degeneracy). In the computation, $\Lambda_x = \Lambda_y = 30\lambda$ and 20λ are chosen for $\Delta n=0.6\%$ and 10%, respectively.

First, examples of convergency of the solutions are shown in Fig.3 when the truncation number M(=N) is increased. As for the eigenvalues of each higher-order mode in the fiber with $\Delta n=0.6\%$, the accuracy of about 6~7 significant figures is expected from the curves of convergencies in Fig.3(a), comparing with the exact values. However, the accuracy of the field distribution is largely decreased to about 2~3 significant figures. It is confirmed that the curves of convergencies for E_x and E_y of HE_{21}^E mode almost lie on those for E_y and E_x of TE_{01} mode, respectively, in the case of $\Delta n=0.6\%$. On the HE_{21}^M mode, they also lie similarly on those of TM_{01} mode. In the case of $\Delta n=10\%$, the curves of convergencies of HE_{21}^E and HE_{21}^M modes vary similarly near those of TE_{01} and TM_{01} modes, respectively. In the computation of the field distributions in Figs.4~6, although the smaller numbers of M than the maximum ones obtained in Fig.3 are chosen for the saving of computational memory and time, the accuracy is considered to be enough to explain qualitatively each problem.

In Fig.4, computed eigenvalues and electric field intensities of E_x and E_y of each mode are shown. First, it is noted that the peak value of E_y component in HE_{11}^x mode is negligibly small, but becomes larger for larger Δn.

Next, as for the TE_{01} mode, it is confirmed that, according to the obtained results computed from the eigenvectors corresponding to the eigenvalue of original TE_{01} mode, the field distribution is expressed by the similar two-lobe patterns as shown in Fig.2, but has slightly different peak values between the field distributions of E_x and E_y as shown in the numerical values in Fig.4(a). This seems to be caused by the admixture of original TE_{01} mode with a small amount of another mode HE_{21}^E which has the same two-lobe pattern as the TE_{01} mode but has slightly different eigenvalue. As the result, new mode TE_{01}' ($\approx TE_{01} + \alpha HE_{21}^E$) appears, and the difference of peak values between E_x and E_y in the new mode occurs according to the small rate α. Due to the similar consideration, there appear $HE_{21}^E{}'$ ($\approx HE_{21}^E - \alpha TE_{01}$), TM_{01}' ($\approx TM_{01} + \alpha' HE_{11}^M$) and $HE_{21}^M{}'$ ($\approx HE_{21}^M - \alpha' TM_{01}$). Here, it is

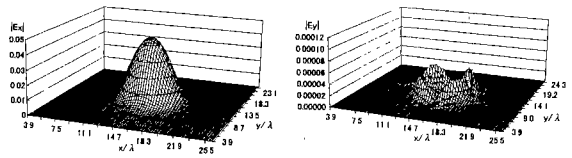

E_x^p=0.044 $E_y^p = 4\times10^{-5}$

HE_{11}^x $\beta/k_0 = 1.45951387$

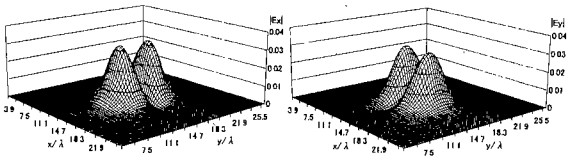

E_x^p=0.03205 E_y^p=0.03061

(=0.03133+0.00072) (=0.03133−0.00072)

$E_x^p - E_y^p$=0.00144 (4.6%)

TE_{01}' $\beta/k_0 = 1.45596916$ $(\approx TE_{01} + \alpha HE_{21}^E)$

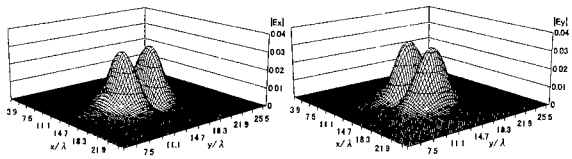

E_x^p=0.03055 E_y^p=0.03200

(=0.03127−0.00072) (=0.03127+0.00072)

$E_x^p - E_y^p$=−0.00145 (4.6%)

$HE_{21}^{E\prime}$ $\beta/k_0 = 1.45595513$ $(\approx HE_{21}^E - \alpha TE_{01})$

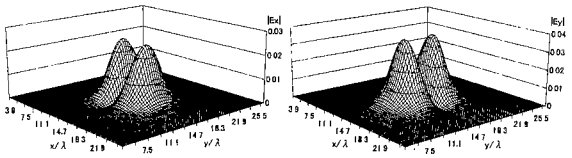

E_x^p=0.02667 E_y^p=0.03513

(=0.03090−0.00423) (=0.03090+0.00423)

$E_x^p - E_y^p$=−0.00846 (27.4%)

TM_{01}' $\beta/k_0 = 1.45595767$ $(\approx TM_{01} + \alpha' HE_{21}^M)$

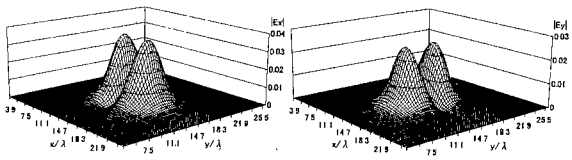

E_x^p=0.03520 E_y^p=0.02676

(=0.03098+0.00422) (=0.03098−0.00422)

$E_x^p - E_y^p$= 0.00844 (27.2%)

$HE_{21}^{M\prime}$ $\beta/k_0 = 1.45595523$ $(\approx HE_{21}^M - \alpha' TM_{01})$

(a) Δn=0.6% (n_c=1.453), $\Lambda_x = \Lambda_y = 30\lambda$, M=N =20

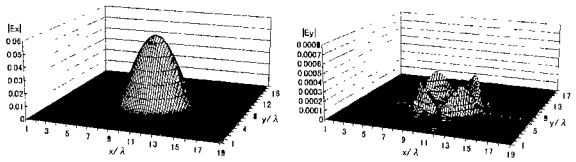

E_x^p=0.056 $E_y^p = 3\times10^{-4}$

HE_{11}^x $\beta/k_0 = 1.45830106$

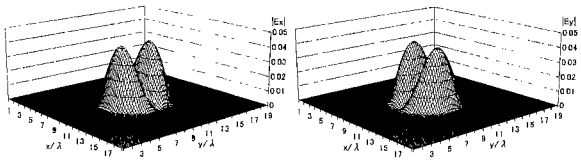

E_x^p=0.04124 E_y^p=0.04088

(=0.04106+0.00018) (=0.04106−0.00018)

$E_x^p - E_y^p$=0.00036 (0.87%)

TE_{01}' $\beta/k_0 = 1.45270187$

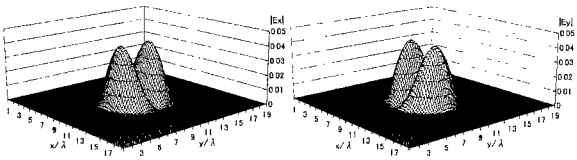

E_x^p=0.04106 E_y^p=0.04142

(=0.04124−0.00018) (=0.04124+0.00018)

$E_x^p - E_y^p$=−0.00036 (0.87%)

$HE_{21}^{E\prime}$ $\beta/k_0 = 1.45259265$

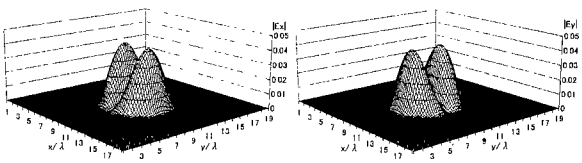

E_x^p=0.04144 E_y^p=0.04084

(=0.04114+0.00030) (=0.04114−0.00030)

$E_x^p - E_y^p$=0.00060 (1.46%)

TM_{01}' $\beta/k_0 = 1.45252021$

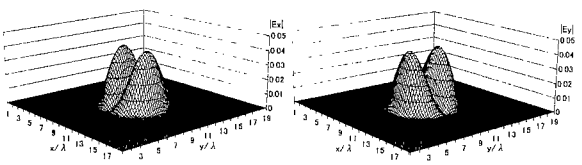

E_x^p=0.04074 E_y^p=0.04134

(=0.04104−0.00030) (=0.04104+0.00030)

$E_x^p - E_y^p$=−0.00060 (1.46%)

$HE_{21}^{M\prime}$ $\beta/k_0 = 1.45259482$

(b) Δn=10% (n_c=1.3158), $\Lambda_x = \Lambda_y = 20\lambda$, M=N =16

Fig.4 Eigenvalues and electric field intensities for each mode in the fiber with the core of r=3.46 λ and n_f=1.462. Numerical values in the parentheses ( ) of $E_x^p - E_y^p$ indicate the value $((E_x^p - E_y^p)/(E_x^p + E_y^p)/2)\times100$.

noted that the new modes TE_{01}' and $HE_{21}^{E}{}'$ (or TM_{01}' and $HE_{21}^{M}{}'$) have the same α (or α') but the opposite sign, respectively, as shown in the numerical examples in Fig.4(a). Referring to the results in Fig.4, it is confirmed that the small ratios α and α' are proportional inversely to the difference of the eigenvalues between the two related modes, and as the difference becomes larger, the difference of peak values $E_x^p - E_y^p$ becomes smaller.

In the case of large Δn in which the modes are already not in degeneracy, the new mode approaches to the original mode itself ($\alpha = \alpha' \sim 0$), then the difference of peak values approaches to zero ($E_x^p - E_y^p \sim 0$). Results for Δn=10% (in Fig.4(b)) may be approximately regarded as such a case.

Thus, the occurrence of the difference in peak values between E_x^p and E_y^p in weakly guiding fiber as shown in Fig.4(a) is considered to be caused by the situation of approximate degeneracy between the related two modes which have the same two-lobe

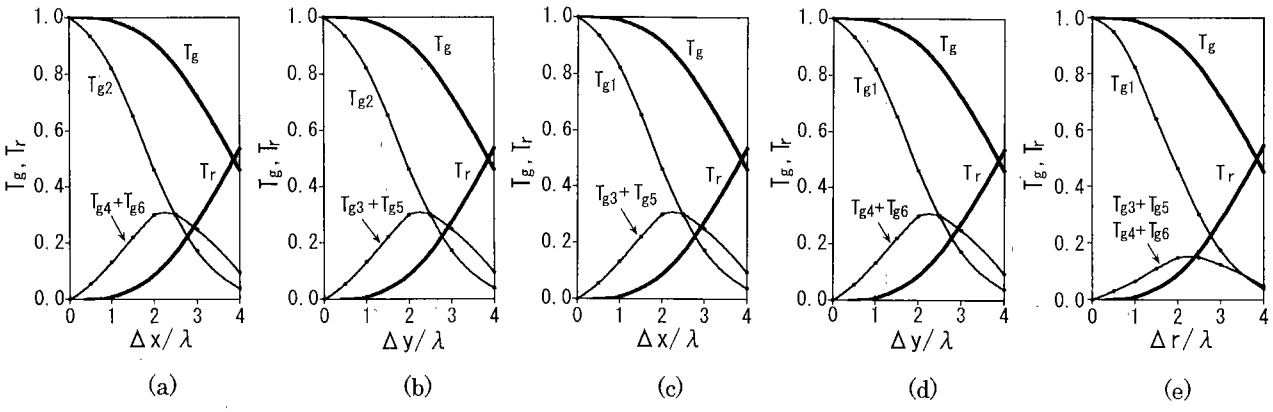

Fig.5. Transmitted powers of each mode for transverse shifts along each axis between two fibers with Δn=10%. Parameters are the same as those of Fig.4(b). Δr is the distance along oblique axis. T_{g1} and T_{g2} are the powers of HE_{11}^{y} and HE_{11}^{x} modes, respectively. (a),(b) : HE_{11}^{x} incidence, (c)~(e) : HE_{11}^{y} incidence.

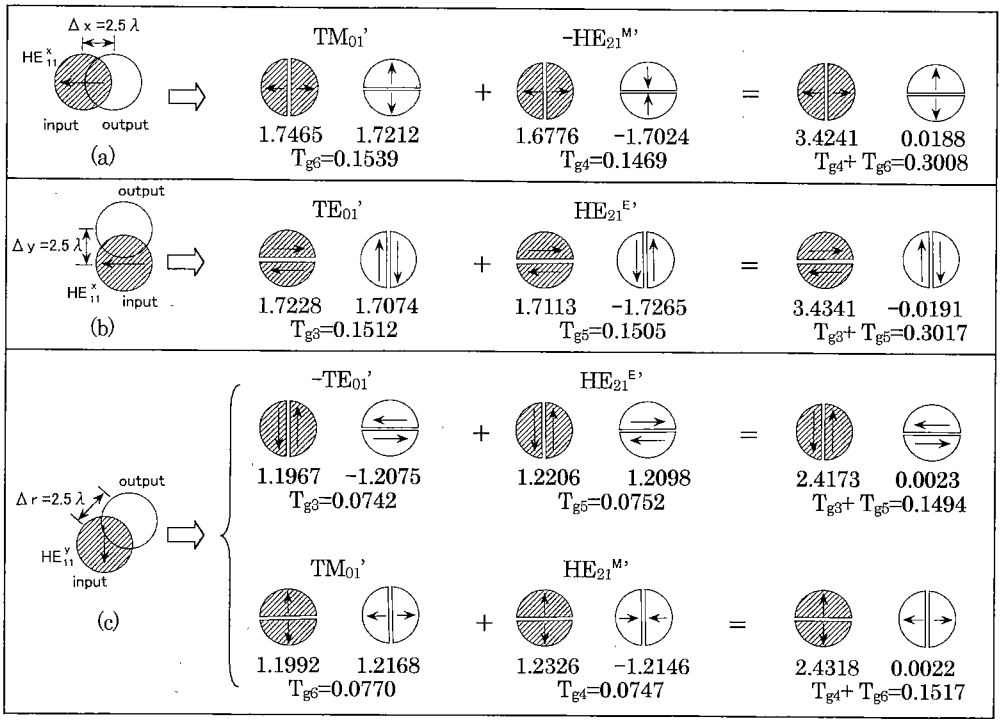

Fig.6. Schematic explanation of the occurrence mechanism of higher-order modes in the output fiber for transverse shifts of Δx, Δy and Δr=2.5λ, referring to the obtained results in Fig.5. Numerical values of under side of the two-lobe patterns indicate calculated peak values of each field. It is noted that the order of higher-order mode in the case of Δn=10% is ③TE_{01}, ④HE_{21}^{M}, ⑤HE_{21}^{E}, ⑥TM_{01} (differ from the order in weakly guiding fiber of Fig.2).

pattern. However, exact solutions for original modes do not have such a difference between E_x^p and E_y^p, even in the weakly guiding fiber. These phenomenon is considered to be peculiar one due to the method used in the present paper, limited to the analysis of the modes in approximate degeneracy. Of course, in the case of no degeneracy, the present method does not have such a problem. We are now trying to obtain the field distribution in the separate original mode, taking the parity, the symmetry of the field distribution and so on into consideration.

4.2 Connection problem of two fibers

In order to explain qualitatively the connection problem between two optical fibers, we choose the step-index type fiber with Δn=10%, which is regarded approximately as the case of no degeneracy and the effect of mode admixture can be neglected ($\alpha, \alpha' \sim 0$ in Fig.4(a)) within the computing accuracy obtained by the present method. In Fig.5, the computed transmitted powers $T_{gk}=\left|a_k^{II+}(z_1)\right|^2$ (k=1,2,⋯,6), T_g and T_r given by Eq.(24) are shown, when the same two fibers with Δn =10% investigated in Fig.4(b) are shifted along x- and y-axes and the oblique axis tilted 45 degree in Fig.1. Here the reflected powers expressed by Eq.(25) are R_g $<10^{-3}$ and R_r $<10^{-4}$, and omitted in Fig.5. It is also confirmed that R_g becomes smaller for smaller Δn. In the case of Δn=10%, many higher-order modes exist. However, in the connection problem, higher-order guided modes, except for TE_{01}, TM_{01}, HE_{21}^E and HE_{21}^M modes, are negligibly small in the output fiber for dominant mode incidence.

In Fig.6, schematic explanation of the occurrence mechanism of the higher-order modes in the output fiber is tried for dominant mode incidence, referring to the obtained peak values E_x^p, E_y^p and powers of each mode for the shifts of Δx, Δy and $\Delta r = 2.5\lambda$. Referring to Figs.5 and 6, the occurrence mechanism of the higher-order modes is explained qualitatively as follows.

First, for HE_{11}^x mode (E_x : dominant) incidence and shift along x-axis, illumination to the half side of the cross section of the output fiber excites the two modes TM_{01}' and HE_{21}^M' which have the same two-lobe pattern of E_x with null line along y-axis, and they are admixed so that the admixed E_y field vanishes. It is noted that, in the numerical results, the sum of E_y field in the output fiber is not zero due to the computing error, but can be neglected practically comparing to the sum of E_x fields. As the result, only the admixed new mode of two-lobe pattern of E_x with null line along y-axis appears in the output fiber with the power of $T_{g4}+T_{g6}$ as shown in Figs.5(a) and 6(a). The other two modes TE_{01}' and HE_{21}^E' do not have the null line along y-axis in the field of E_x (see Fig.6(b), Fig.2), then they can not be excited in the output fiber in this case. Next, for the shift along y-axis, according to the similar consideration, TE_{01}' and HE_{21}^E' are admixed, and the two-lobe pattern of E_x with null line along x-axis appears with the power of $T_{g3}+T_{g5}$ (see Fig.5(b), Fig.6(b)).

For HE_{11}^y mode (E_y : dominant) incidence and shift along x-axis, similarly, TE_{01}' and HE_{21}^E' which have the same two-lobe pattern of E_y with null line along y-axis are admixed so that the admixed E_x field vanishes. Then the two-lobe pattern of E_y with null line along y-axis appears with the power of $T_{g3}+T_{g5}$ (see Fig.5(c), upper part of Fig.6(c)).

Lastly, for HE_{11}^y mode incidence and shift along oblique axis tilted 45 degree, due to the illumination to the third quadrant of the cross section of the output fiber, two sets of admixed modes are excited in the output fiber. That is, TE_{01}' and HE_{21}^E' which have the same two-lobe pattern of E_y with the null line along y-axis, and TM_{01}' and HE_{21}^M' which have the same two-lobe pattern of E_y with null line along x-axis are all excited and admixed with the powers of $T_{g3}+T_{g5}$ and $T_{g4}+T_{g6}$, respectively (see Fig.5(e), Fig.6(c)).

5. Conclusion

Fourier series expansion method is applied for full-vectorial analysis of optical fiber and connection problem of the two fibers. First, accuracy for obtained results is examined briefly. Then the computed eigenvalues and field distributions of higher-order modes obtained by the proposed method are shown in detail for the two cases of Δn=0.6% (weakly guiding fiber) and Δn=10%. In the former case, it is confirmed that the field distributions of each mode in LP_{11} mode obtained by the present method are admixed with a small amount of another mode which has the similar two-lobe pattern, according to the degree of degeneracy. Then different peak values appear between E_x and E_y. These differences approach to zero as Δn becomes larger. Such a phenomenon in the weakly guiding fiber is considered to be a peculiar one to the present method, limited to the analysis of the LP_{11} mode which is in approximate degeneracy. For further investigation of such a case, we are now trying to improve our present method to separate such an admixture of the related two modes in approximate degeneracy, taking the parity and symmetry of the field into consideration.

In the connection problem of the two fibers with Δ

n=10% in which the effect of the degeneracy mentioned above can be neglected, mechanism of the occurrence of the higher-order modes is made clear in detail, for the transverse shifts of the two fibers. It is confirmed that the kind of the higher-order mode which appear in the output fiber can be predicted qualitatively according to the polarization of the incident wave and the direction of the shift between two fibers.

(Manuscript received January 26, 2001, revised manuscript received August 1, 2001)

References

(1) E. Snitzer, "Cylindrical dielectric waveguide modes", *J. Opt. Soc. Am.*, Vol.51, No.5, pp.491-498 (1961).

(2) E. Snitzer, and H.Osterberg, "Observed dielectric waveguide modes in the visible spectrum", *J. Opt. Soc. Am.*, Vol.51, No.5, pp.499-505 (1961).

(3) T. Ookoshi, ed., Fundamentals of optical fibers, Ohmsha, Ltd., 1977. (in Japanese)

(4) D. Marcuse, "Solution of the vector wave equation for general dielectric waveguides by the Galerkin method", *IEEE J. Quant. Electr.*, Vol.28, No.2, pp.459-465 (1992).

(5) T. Hosono, T. Hinata, and A. Inoue, "Numerical analysis of the discontinuities in slab dielectric waveguides", *Radio Science*, Vol.17, No.1, pp.75-83 (1982).

(6) J. Yamakita, K. Matsumoto, and K. Rokushima, "Analysis of discontinuities in anisotoropic dielectric waveguides", IEICE Technical Report, EMT-93-87, pp.81-89 (1993). (in Japanese)

(7) Y. Yasumoto, and K. Ohzawa, "Analysis of a step transition in optical fiber using periodic boundary conditions", Asia-Pacific Microwave Conference Proc., pp.665-668 (1997).

(8) T. Miyamoto, M. Momoda, and K. Yasumoto, "Analysis of an embedded dielectric waveguide with parabolic index distribution in the two-dimensional cross section", 1998 Int. Conf. on Microwave and Millimeter wave Technology Proc., pp.841-844 (1998).

(9) M. Momoda, T. Miyamoto, and K. Yasumoto, "Analysis on connection problem of three-dimensional optical waveguides using Fourier series expansion method (II)", IEICE Technical Report, EMT-99-65, 65-71 (1999). (in Japanese)

(10) M. Momoda, T. Miyamoto, and K. Yasumoto, "Full-vectorial analysis on field distributions of higher-order mode (EH_{11}) in optical fiber", IEICE Technical Report, OPE2000-89, pp.53-58 (2000). (in Japanese)

(11) T. Miyamoto, M. Momoda, and K. Yasumoto, "Mechanism of higher-order mode occurrence due to the shift of the center axis in the connection of optical fibers", IEICE Technical Report, EMT-00-106, pp.43-48 (2000). (in Japanese)

Tokuo Miyamoto (Non-member) received the B.E. degree from Tokushima University, Tokushima, Japan in 1963, and the D.E. degree from Kyushu University, Fukuoka, Japan in 1978. He was a research assistant at Kyushu University from 1963 to 1970. He joined the Faculty of Engineering of Fukuoka University, Fukuoka, Japan in 1970, where he has been a professor since 1976. He has engaged in research on Laser resonator and beam, numerical analyses of elastic waveguide and optical waveguide. He is a member of IEICE of Japan, Japan Applied Physics Society, Optical Society of America.

Michiko Momoda (Non-member) received the B.S. degree from Fukuoka University, Fukuoka, Japan in 1979. From 1979 she has worked at Fukuoka University as a research assistant, and engaged in research on numerical analysis on optical waveguide. She is a member of IEICE of Japan.

Kiyotoshi Yasumoto (Member) received the B.E., M.E. and D.E. degrees from Kyushu University, Fukuoka, Japan in 1967, 1969 and 1977, respectively. He joined the Faculty of Engineering of Kyushu University in 1969, where he has been a professor since 1988. His research interests are in electromagnetic wave theory and its application to microwave and optical waveguides. He is a member of IEICE of Japan, Optical Society of America, Electromagnetic Academy at MIT, a senior member of IEEE, and a fellow of CIE.